

**DISPERSION OF IRON OXIDE NANOPARTICLES ON OXIDE  
NANOTUBE FOR NANOCATALYST SYSTEM**

by

DEDE MIFTAHUL ANWAR

**Thesis submitted in fulfilment of the requirements  
for the degree of Master**

**June 2014**

## ACKNOWLEDGEMENTS

Syukur Alhamdulillah to Allah SWT for the completion of this study.

First of all, I would like to express my deepest gratitude to my supervisor, Assoc. Prof. Dr. Zainovia Lockman for her guidance, encouragement, and assistance throughout my study. I would also like to extend my appreciation to Assoc. Prof. Dr. Khairunisak Abd. Razak as my co-supervisor for her advice and valuable input regarding my work at Universiti Sains Malaysia. I am also taking this opportunity to humbly apologize to both of them for any inconvenience I have unintentionally caused them.

Special acknowledgement is also extended to Assoc. Prof. M. Waziz Wildan, Faculty of Engineering, Universitas Gadjah Mada, Professor Atsunori Matsuda and Assistant Professor Go Kawamura, Department of Electrical and Electronic Information Engineering, Toyohashi University of Technology for the assistance and support in this research.

I have to acknowledge AUN/SEED-Net/JICA and Long Term Research Grant (LRGS) with Universiti Teknologi Petronas Malaysia under OneBaja Project for the financial support. I would like to express my gratitude to AUN/SEED-Net Chief Advisor, Prof. Dr. MIKI Chitosh, and Program Officer for USM, Ms. Natechanok Sarakoses and also Mrs. Irda and Mrs. Norpisah from USM for their kind support and assistance.

Furthermore, I am thankful to the Dean of PPKBSM, Prof. Hanafi Ismail, Deputy Dean, Prof. Zainal Arifin Ahmad and to Professor Radzali Othman, Prof. Dr. Ir Mariatti Jaafar and Profesor Ahmad Fauzi Mohd Noor. Not forgetting all the respective lecturers, staff and technicians of School of Material and Mineral Resources Engineering, thank you for the help given, either directly or indirectly.

A special thank you goes to GEM groupies; Syahriza, Azhar, Monna, Faisal, Ehsan, Cha Yan, Qurratu Aini for their help in the laboratory. My sincere thanks also extended to all PPI member; Mas Syukron, Pa Dodi, Pa Indra, Pa Teguh, Pa Janter, Pa Syamsudin, Pa Syafrudin, Bu tuti, Pa Suryadi for great support, invaluable advice and great companion.

To my parents, ummi Aah and Abi Anwar, I can never fully repay their love and endless support. I am deeply indebted to them and I truly wish that I have made them proud. To my beloved wife, Ari Purwani and my daughters, Hafidzah Miftahul Firdausi and Zakira Miftahul Raudhati, thank you for being here for me. You kept me going even when I was ready to give up. I love you all. Finally, to all my friends in PG room, your contributions are very much appreciated and the wonderful time I've spent with all of you will be remembered always.

Dede Miftahul Anwar

25 June 2014

## TABLE OF CONTENTS

DECLARATION .....	i
ACKNOWLEDGEMENTS .....	ii
TABLE OF CONTENTS .....	iv
LIST OF TABLE .....	vii
LIST OF FIGURE.....	viii
LIST OF ABBREVIATIONS .....	xiii
LIST OF SYMBOLS .....	xiv
LIST OF PUBLICATIONS .....	xvi
ABSTRAK .....	xviii
ABSTRACT.....	xx
1 CHAPTER 1 INTRODUCTION.....	1
1.1 Introduction .....	1
1.2 Problem statement .....	5
1.3 Objectives .....	8
1.4 Thesis outline.....	8
2 CHAPTER 2 LITERATURE REVIEW.....	10
2.1 Introduction .....	10
2.2 Valve metal oxide.....	10
2.2.1 Metal oxide nanotube arrays.....	10
2.2.1.1 Properties of TiO <sub>2</sub> nanotubes .....	12
2.2.1.2 Properties of ZrO <sub>2</sub> Nanostructure .....	16
2.2.2 Synthesis Metal Oxide Nanotube arrays by Anodization.....	18
2.2.3 Factor affecting geometry and composition .....	18
2.2.3.1 Effect of Electrolyte composition (nanotube arrays synthesis using organic electrolyte).....	19
2.2.3.2 Effect of applied voltage.....	28

2.2.3.3	Effect of fluoride concentration.....	30
2.2.3.4	Effect of anodization time .....	31
2.3	Hybrid nanostructures .....	33
2.3.1	Catalyst and Catalysts Support .....	33
2.3.2	Photocatalyst.....	35
2.3.3	Photoelectrochemical.....	37
2.3.4	Nobel Metal Loading .....	39
2.3.5	Metal Ion Doping.....	41
2.3.6	Composite Semiconductors .....	42
2.3.7	Electrodeposition to synthesis hybrid nanostructured .....	45
2.3.7.1	Migration .....	48
2.3.7.2	Diffusion.....	48
2.3.7.3	Convection.....	51
2.3.7.4	Formation of oxide via electrogeneration of base .....	51
3	CHAPTER 3 METHODOLOGY.....	54
3.1	Introduction .....	54
3.2	Raw materials and chemicals .....	54
3.3	Experimental design .....	56
3.3.1	Formation of metal oxide nanotubes arrays as a template for electrodeposition.....	57
3.3.2	Formation of hybrid photocatalyst system .....	58
3.4	Experimental procedure of experiment .....	60
3.4.1	Formation of metal oxide nanotube .....	60
3.4.2	Improvement of structural characteristic of metal oxide nanotube by the addition of various oxidants.....	62
3.4.3	Formation of hybrid photocatalyst system by electrodeposition...	62
3.5	Characterization techniques.....	63
3.5.1	Field Emission Scanning Electron Microscopy (FESEM) .....	63
3.5.2	Energy Dispersive X-ray spectroscopy (EDX).....	64
3.5.3	X-ray Diffraction spectrometry (XRD) .....	65
3.5.4	Transmission Electron Microscopy (TEM) .....	66
3.5.5	Raman spectroscopy .....	68
3.5.6	Potentiodynamic polarization .....	69

3.5.7	Electrochemical impedance spectroscopy .....	70
3.5.8	AC impedance analysis.....	71
3.5.9	Mott-schottky analysis.....	72
3.5.10	UV-Visible Spectroscopy .....	73
3.5.11	Photodegradation .....	74
4	CHAPTER 4 RESULT AND DISCUSSION .....	76
4.1	Introduction .....	76
4.2	Formation of metal oxide nanotube arrays .....	76
4.2.1	TNT and ZNT arrays formation .....	77
4.2.1.1	Polarization.....	91
4.2.1.2	Charge carrier .....	95
4.3	Development of TNT arrays by incorporating KOH, H <sub>2</sub> O and H <sub>2</sub> O <sub>2</sub> .....	98
4.3.1	Growth behaviour .....	99
4.3.2	Morphology .....	101
4.3.3	Polarization .....	106
4.3.4	Electrochemical Impedance Spectroscopy .....	109
4.3.5	Crytal Structure.....	113
4.4	Formation of hybrid nanotube arrays (Fe <sub>2</sub> O <sub>3</sub> on KOH TiO <sub>2</sub> ).....	116
4.4.1	Growth mechanism of electrodeposition of Iron oxide .....	118
4.4.2	Effect of voltage on electrodeposition of Iron oxide on TNT .....	129
4.4.3	Effect of additive .....	132
4.5	Properties of Hybrid: Iron Oxide TNTs.....	134
4.5.1	Photodegradation .....	134
4.5.2	Photoelectrochemical properties.....	136
4.5.2.1	Photocurrent.....	136
4.5.2.2	Mott-Schottky analysis .....	137
5	CHAPTER 5 CONCLUSION AND SUGGESTIONS .....	141
5.1	Conclusion.....	141
5.2	Suggestion for future research work.....	144
6	REFERENCES.....	145

## LIST OF TABLE

Table 2.1	Summary of the nanotube inner diameter, outer diameter, and length obtained at different voltages for a 17 h anodization in a fresh, un-used ethylene glycol electrolyte containing 0.3 wt% $\text{NH}_4\text{F}$ and 2 vol% $\text{H}_2\text{O}$ (Prakasam <i>et al.</i> , 2007).	29
Table 3.1	Raw materials and chemicals used for the preparation of template nanotube arrays, the fabrication for hybrid photocatalyst system, as well as photocatalytic performance evaluation	55
Table 3.2	The variable and constant parameters for the formation of template nanotube arrays for electrodeposition The variable and constant parameters for the formation of template nanotube arrays for electrodeposition	58
Table 3.3	The variable and constant parameters for the formation of template nanotube arrays for electrodeposition	60
Table 4.1	Structural characteristics of TNTs and ZNTs prepared in EG containing 0.5 wt % $\text{NH}_4\text{F}$ at 60 V for 30 min.	90
Table 4.2	Parameters derived from potentiodynamic polarization curve for TNT and ZNT	93
Table 4.3	Structural characteristics of TNT arrays in EG containing 0.5 wt % $\text{NH}_4\text{F}$ and with the addition of 1 vol % $\text{H}_2\text{O}$ , $\text{H}_2\text{O}_2$ and $\text{KOH}$ at 60 V for 30 min.	103
Table 4.4	Parameters derived from potentiodynamic polarization curve for TNT fabricated in different oxidation agent.	107
Table 4.5	Electrochemical factors from the complex impedance spectra, and calculated ionic conductivities of EG electrolytes containing 0.5 wt % $\text{NH}_4\text{F}$ and different contents of oxidant at room temperature.	111
Table 4.6	The possible peak of electrodeposited sample	123
Table 4.7	The possible raman shift of TNT arrays deposited sample by iron oxide	126

## LIST OF FIGURE

Figure 1.1	Illustration of a structured photocatalyst system	4
Figure 2.1	Glancing angle X-ray diffraction (GAXRD) patterns of TiO <sub>2</sub> nanotube arrays annealed at temperatures range from 230 to 880°C for 3 h. A, R, and T represent anatase, rutile, and titanium, respectively (Varghese et al., 2003).	14
Figure 2.2	Illustrative drawing of a two-electrode electrochemical cell in which the valve metal are anodized.	18
Figure 2.3	Different morphologies of the oxides obtained by anodization of transition metals in various electrolytes: (a) barrier type-oxide can be formed in most of the aqueous electrolytes, (b) mesosponge, microcones, nanochannels formed in hot-glycerol phosphate electrolyte, (c) nanotubes formed in fluoride electrolytes, and (d) oxide with open porous character	21
Figure 2.4	FESEM images of a nanotube arrays grown in ethylene glycol containing 0.25wt % NH <sub>4</sub> F at 60 V showing (a-d) cross-sectional views at varying degrees of magnification, (e) view of bottom surface and (f) top surface (Prakasam <i>et al.</i> , 2007)	23
Figure 2.5	Top view (left) and cross-sectional view (right) of FESEM images of TiO <sub>2</sub> nanotubes fabricated in ethylene glycol electrolyte containing 5 wt % NH <sub>4</sub> F with: (a) 1 wt%; (b) 3 wt%; (c) 5 wt% ; and (d) 10 wt% H <sub>2</sub> O <sub>2</sub> addition at 60 V for 1h (Sreekantan <i>et al.</i> , 2010)	25
Figure 2.7	Cross sectional images of anodised zirconium foils in electrolyte containing (a) 0.1 g, (b) 0.5 g and (c) 0.7 g NH <sub>4</sub> F in 100 nm 85% glycerol at 30 V. Insets are the surface morphologies (Lockman et al., 2011)	27
Figure 2.7	Illustration and SEM sequence for difference stage of TiO <sub>2</sub> nanotubes formation (a) 0 min (b) 3 min (c) 10 min (d) 30 min and (e) 60 min (Macak et al., 2008)	32
Figure 2.9	Various schemes illustrating the possible band-gap electronic structure and excitation processes of visible light responsive TiO <sub>2</sub> : (a) pure TiO <sub>2</sub> , (b) doped TiO <sub>2</sub> with localized dopant levels near the VB and the CB, (c) band-gap narrowing model of nonmetal doped TiO <sub>2</sub> , (d) localized dopant levels and electronic transitions to the CB and (e) electronic transitions from localized levels	38



near the VB to their corresponding excited states for  $Ti^{3+}$  and  $F^+$  centres (Fujishima et al., 2008).

Figure 2.10	Schematic illustration of electron energy associated with the sacrificial electron donor	39
Figure 3.1	Flow chart presents the overall methodology for the formation of hybrid photocatalyst system	56
Figure 3.2	Flow chart presents the formation of metal oxide nanotubes arrays as a template for electrodeposition	57
Figure 3.3	Flowchart presents the formation of hybrid photocatalyst system	59
Figure 3.4	Flow chart for procedures of experiment	60
Figure 3.5	Schematic illustration of equipment and setup in anodization process	61
Figure 3.6	Heating profile of the annealing	63
Figure 3.7	Bragg scattering. The constructive interference gives the pattern to the diffraction and occur when the scattered waved is an integer multiple of wavelength $\lambda$ (Stanjek and Häusler, 2004).	66
Figure 3.8	Mechanism in Raman spectroscopy	68
Figure 3.9	Schematic plot of a potentiodynamic polarisation curve	70
Figure 4.1	J-t curve during anodization of the Ti metal in EG electrolyte containing 0.5 wt% $NH_4F$ at 60 V for 30 min. The inset shows the magnified J-t curve in the range of 0 – 5 min.	78
Figure 4.2	a) Schematic drawing showing field-aided transport of mobile ions through the oxide layers in the absence and (b) presence of fluoride ions.	79
Figure 4.3	FESEM images of oxide layers after exposure to EG electrolyte containing 0.5 wt. % $NH_4F$ at 60 V for (a) 30 s, (b) 1, (c) 3, (d) 5, (e) 10 and (f) 30 min. The insets show the cross-sectional morphologies.	80

Figure 4.4	The evolution of nanotube arrays under potentiostatic: (a) oxide layer formation, (b) pit formation of the oxide layer, (c) growth of the pit into scallop shaped pores, (d) fully developed nanotube array with a corresponding top view, (e) schematic drawing of tube/pore evolution from small to large tube/pore. The magnified image shows the ionic mobility at the oxide/electrolyte interface as well as the typical dissolution during anodization at the pore bottom ( $D_1$ ), surface ( $D_2$ ) and interpore ( $D_3$ ).	84
Figure 4.5	$J$ - $t$ curve during anodic oxidation of the Zr metal in EG electrolyte containing 0.5 wt % $\text{NH}_4\text{F}$ at 60 V for 30 min. the inset shows the magnification at 0 - 3.5 min.	86
Figure 4.6	FESEM images of $\text{ZrO}_2$ after anodization in EG electrolyte containing 0.5 wt% $\text{NH}_4\text{F}$ at 60 V for (a) 5, (b) 10, and (c) 30 min. Images with (i) are the surface morphologies and (ii) are the cross-sectional morphologies.	88
Figure 4.7	Potentiodynamic polarization curve for (a) $\text{TiO}_2$ and (b) $\text{ZrO}_2$ in ethylene glycol electrolyte containing 0.5 g $\text{NH}_4\text{F}$ . (c) is the combination of both graphs (a) and (b)	92
Figure 4.8	(a) Photocurrent density versus applied potential curve under visible light illumination and (b) Charge versus applied potential curve under visible light illumination for (i) TNT and (ii) ZNT. (c) and (d) are the magnification for ZNT curve	96
Figure 4.9	$J$ - $t$ curves during anodization of the Ti metals in (a) EG electrolytes containing 0.5 wt% $\text{NH}_4\text{F}$ and with the addition of (b) 1 wt% $\text{H}_2\text{O}$ , (c) 1wt% $\text{H}_2\text{O}_2$ and (d) 1 wt% $\text{KOH}$ at 60 V for 30 min. The insets show the magnification of $J$ - $t$ curves in the range of 0 – 5 min	100
Figure 4.10	FESEM images of anodized Ti in (a) EG electrolyte containing 0.5 wt% $\text{NH}_4\text{F}$ and with the addition of 1 wt% (b) $\text{H}_2\text{O}$ , (c) $\text{H}_2\text{O}_2$ and (d) $\text{KOH}$ at 60 V for 30 min. The insets show the cross-sectional morphologies	102
Figure 4.11	Potentiodynamic polarization curve of $\text{TiO}_2$ in (a) EG and with the addition of 1 vol% (b) $\text{H}_2\text{O}$ , (c) $\text{H}_2\text{O}_2$ and (d) $\text{KOH}$	107

Figure 4.12	Complex impedance spectra of (a) EG electrolytes containing 0.5 wt% $\text{NH}_4\text{F}$ , and with addition of (b) 1 wt% $\text{H}_2\text{O}$ , (c) 1wt% $\text{H}_2\text{O}_2$ and (d) 1wt% $\text{KOH}$ .	110
Figure 4.13	Equivalent circuit for the complex impedance spectra of TNT arrays formation	111
Figure 4.14	X-ray diffraction patterns of as-anodised Ti in fluoride (a) EG (b) EG + $\text{H}_2\text{O}$ , (c) EG + $\text{H}_2\text{O}_2$ and (d) EG + $\text{KOH}$ electrolyte	113
Figure 4.15	Raman spectra of as-grown nanotube arrays prepared in (a) EG containing 0.5 wt% $\text{NH}_4\text{F}$ and with the addition of (b) 1wt% of $\text{KOH}$ , (c) 1wt% of $\text{H}_2\text{O}$ and (d) 1wt% of	115
Figure 4.16	Current density Vs time during electrodeposition process of TNT in $\text{FeCl}_3 \cdot 6\text{H}_2\text{O}$ / Glycerol at -3 V for 30 min	118
Figure 4.17	FESEM images of (a) as anodized TNTs fabricated in EG + $\text{KOH}$ electrolyte and electrodeposited iron oxide in 0.02 M $\text{FeCl}_3$ / glycerol (b) before and (c) after annealing at $450^\circ\text{C}$ for 2h.	121
Figure 4.18	XRD pattern of TNT nanotube arrays (a) before and (b) after depositing iron oxide at -3V for 30 min.	123
Figure 4.19	(a) Raman spectra of TNT arrays deposited sample by iron oxide annealed at $450^\circ\text{C}$ for 2 h in air. (b) is the magnification at the range of $100\text{-}450\text{ cm}^{-1}$	125
Figure 4.20	(a) HRTEM image of TNT nanotube array deposited iron oxide by electrodeposition at -3V for 30 min. (b) the magnification image and the inset shows the SAED patterns.	126
Figure 4.21	EDX mapping from HRTEM of TNTs electrodeposited sample in 0.02M $\text{FeCl}_3 \cdot \text{H}_2\text{O}$ /glycerol at -3V for 30 min	128
Figure 4.22	TEM and HRTEM images of TNTs electrodeposited in 0.02M $\text{FeCl}_3 \cdot 6\text{H}_2\text{O}$ at (a) -1V, (b) -3 V and (c, d) -5 V for 30 min.	129
Figure 4.23	SEM top-view micrographs of samples electrodeposited in water/glycerol/0.02 M $\text{FeCl}_3 \cdot 6\text{H}_2\text{O}$ for 30 min at (a)	130

–1 V, (b) –3 V, (c) –5 V) indicate the rice-like structures formed in certain area on TiO<sub>2</sub> nanotube surface

Figure 4.24	FESEM images of electrodeposited iron oxide in 0.02 M FeCl <sub>3</sub> .6H <sub>2</sub> O solution diluted in (a) DI water, (b) Glycerol, (c) DMSO and (d) Methanol	133
Figure 4.25	Photodegradation of MO (a) without any TNT presents, (b) with presence of TNTs prepared in KOH and hybrid photocatalyst prepared in the addition of (c) methanol, (d) DMSO, (e) Glycerol additive.	135
Figure 4.26	<i>J<sub>p</sub></i> transient curves of TNT electrodeposited iron oxide in the electrolyte containing 0.02 M FeCl <sub>3</sub> .6H <sub>2</sub> O with the mixture of 50 vol% of (a) glycerol, (b) DMSO, (c) DI water and (d) methanol under stimulated solar illumination.	136
Figure 4.27	MS spectra of (a) TNT prepared in EG KOH addition and hybrid nanotube arrays prepared in FeCl <sub>3</sub> .6H <sub>2</sub> O with different additive addition; (b) 50 vol% of DMSO, (c) 50 vol% of Glycerol, (d) 50 vol% of H <sub>2</sub> O and (e) 50 vol% of Methanol	138

## LIST OF ABBREVIATIONS

ZNTs	Zirconium oxide nanotubes
TNTs	Titanium oxide nanotubes
AOPs	Advanced oxidation processes
EIS	Electrochemical impedance spectroscopy
MO	Methyl orange
EG	Ethylene Glycol
PEC	Photoelectrochemical
PC	Photocatalytic
SEM	Scanning Electron Microscopy
FESEM	Field Emission Scanning Electron Microscopy
XRD	X-ray Diffraction
TEM	Transmission Electron Microscopy
HRTEM	High Resolution Transmission Electron Microscopy
MS	Mott-Schottky

## LIST OF SYMBOLS

[ ]	Concentration
cm	Centimetre
h	Hour
L	Litre
m	Meter
min	Minute
mL	Millilitre
mm	Millimetre
rmp	Voltage rate per second
wt %	Weight percent
A	Ampere
V	Voltage
nm	Nanometer
g	Gram
s	Second
eV	Electron volt
$\lambda$	Wavelength
T	Temperature
$D_1$	Chemical dissolution at the pore bottom
$D_2$	Chemical dissolution at the surface
$D_3$	Chemical dissolution of fluoride rich region at the interpore

$L$	Nanotube length
$a$	Diameter of tube
$w$	Wall thickness
$E_{corr}$	Corrosion potential
$J_{corr}$	Corrosion current density
$R_p$	Polarization resistance
$R_s$	Solution resistance
$E_c$	Critical pitting corrosion
$E_{pp}$	Passivation potential
$W$	Warburg impedance
$\sigma$	Ionic conductivity
AR	Aspect ratio
$\mu$	Growth rate
G	Roughness factor

## LIST OF PUBLICATIONS

### International journals

1. Lockman, Zainovia, D. Miftahul Anwar, Monna Rozana, Syahriza Ismail, Ehsan Ahmadi, Abdul Razak Khairunisak, and Kuan Yew Cheong. "Formation of Anodic Oxide Nanotubes in H<sub>2</sub>O<sub>2</sub>-Fluoride Ethylene Glycol Electrolyte as Template for Electrodeposition of  $\alpha$ -Fe<sub>2</sub>O<sub>3</sub>." *Advanced Materials Research* 832 (2014): 333-337.

### Proceeding

1. Dede Miftahul Anwar, Matsuda Atsunori, Go Kawamura, Khairunisak Abdul Razak, Waziz Wildan, Kuan Yew Cheong and Zainovia Lockman, (2011), *Formation of Oxide Nanotubes as Catalysts Support for Ammonia Production*, Conference paper on The First oneBaja Colloquium, 22-25.
2. Dede Miftahul Anwar, Siti N. Qurratu Aini, Matsuda Atsunori, Go Kawamura, Khairunisak Abdul Razak , Waziz Wildan, Kuan Yew Cheong and Zainovia Lockman, (2011), *Titanium Dioxide Nanotubes as Catalyst Support Formed by Anodic Process*, Conference paper on 20<sup>th</sup> Scientific Conference of the Microscopy Society of Malaysia (EMSM), 42
3. Zainovia Lockman, Syahriza Ismail, Dede Miftahul Anwar, (2011), *Formation of Oxide Nanotubes: Review*, Conference paper on The First oneBaja Colloquium, 26-30.



4. **Dede Miftahul Anwar**, Matsuda Atsunori, Go Kawamura, Khairunisak Abdul Razak, Waziz Wildan, Kuan Yew Cheong and Zainovia Lockman, (2012), *Formation of Fe Nanoparticles on Anodically Grown Zirconia and Titania Nanotubes in Peroxide-Organic Electrolyte*, Conference paper on 21<sup>st</sup> Scientific Conference of the Microscopy Society of Malaysia (EMSM), 56
5. **D. Miftahul Anwar**, Khairunisak Abdul Razak, Cheong Kuan Yew, Monna Rozanna and Zainovia Lockman, (2013), *Iron Oxide Nanoparticles Dispersion on Titanium Oxide Nanotubes*, Conference paper on International Conference on Materials for Advanced Technologies (ICMAT)

# **PENYEBARAN BUTIRAN NANO BESI OKSIDA PADA TIUB NANO OKSIDA UNTUK SISTEM PEMANGKIN NANO**

## **ABSTRAK**

Tatasusun nanotiub titanium oksida,  $\text{TiO}_2$  (TNTs) dan zirkornia,  $\text{ZrO}_2$  (ZNTs) telah berjaya dihasilkan dengan penganodan dalam etilena glikol (EG) yang mengandungi 0.5 wt%  $\text{NH}_4\text{F}$  pada 60 V selama 30 minit. Bagi pembentukan nanotiub; pengoksidaan dan keterlarutan telah dikenal pasti sebagai dua proses terpenting. Proses keterlarutan berlaku pada permukaan oksida, di dalam liang dan di antara liang. Untuk membandingkan antara penghasilan TNT dan ZNT struktur adalah didapati ZNT lebih panjang dengan diameter lebih kecil dan dinding nanotiub yang nipis berbanding TNT. Walaupun lapisan tindak balas anod pada Zr mempunyai nilai rintangan pengkutuban yang lebih tinggi ( $\sim 3.92 \text{ k}\Omega$ ) berbanding TNTs ( $\sim 7.82 \text{ k}\Omega$ ), kadar keterlarutan  $\text{ZrO}_2$  lebih rendah (0.11 mm / tahun), berbanding dengan TNT (0.416 mm / tahun), Membuatkan TNTs menjadi lebih pendek. Kadar keterlarutan oksida pada Ti dan Zr yang berbeza juga memberi kesan pada perbezaan panjang dan diameter tiub. Pengukuran arusfoto dan taburan cas menunjukkan keupayaan yang baik untuk pengaliran cas pembawa bebas yang terhasil dari foto bagi TNTs tetapi rendah untuk ZNTs. Oleh itu, TNTs telah dipilih sebagai bahan katod untuk elektroenapan besi oksida. Pertumbuhan TNTs telah dikaji lebih lanjut dengan penambahan pelbagai oksidan ( $\text{H}_2\text{O}$ ,  $\text{H}_2\text{O}_2$  dan  $\text{KOH}$ ) ke dalam fluorida-EG. Antara oksidan ini,  $\text{KOH}$  muncul sebagai oksidan terbaik untuk menghasilkan tatasusunan nanotiub dengan kadar  $\sim 254 \text{ nm min}^{-1}$  dan sesuai digunakan sebagai templat elektroenapan. Untuk elektroenapan, elektrolit yang terdiri daripada 0.02 M  $\text{FeCl}_3 \cdot 6\text{H}_2\text{O}$  + air DI digunakan. Parameter yang dikaji untuk proses ini termasuklah

voltan, kepekatan elektrolit dan kesan bahan tambah dalam elektrolit. Mekanisma pertumbuhan nanopartikel dan morfologi diterangkan. Berdasarkan imej mikroskop, kehadiran nano partikel halus dilihat pada permukaan TNTs daripada enapan dalam elektrolit yang ditambah dengan gliserol. Taburan ketumpatan partikel yang lebih tinggi didapati dengan meningkatkan kadar keupayaan tindak balas katod Ti. Saiz dan bentuk nanopartikel juga meningkat dengan voltan yang digunakan. Purata diameter nanopartikel berbentuk sfera yang dihasilkan pada  $-1.0\text{ V}$  adalah  $\pm 41.7\text{ nm}$ . Peningkatan voltan kepada  $-3.0\text{ V}$  menyebabkan morfologi nanopartikel kelihatan seperti struktur beras dengan purata diameter dan panjang adalah  $\pm 44.0\text{ nm}$  dan  $130.0\text{ nm}$  masing-masing. Pembelauan sinar-X (XRD) dan ukuran spektroskopi Raman menunjukkan nanopartikel terdiri daripada magnetit ( $\text{Fe}_3\text{O}_4$ ), maghemit ( $\gamma\text{-Fe}_2\text{O}_3$ ) dan hemetit ( $\alpha\text{-Fe}_2\text{O}_3$ ) selepas penyepuhlindapan pada  $450^\circ\text{C}$  untuk 2 jam (udara). Ukuran fotorosotaan mengesahkan sifat-sifat fotopemangkin nano hibrid terhasil kemerosotan 90% kepekatan logam jingga (MO) terlihat pada system nanopartikel - TNTs berbanding pada TNTs bersih,  $\sim 75.0\%$ . Arusfoto pengukuran menunjukkan sampel ini mempunyai arusfoto yang tinggi ( $\sim 35.0\text{ mA cm}^{-2}$ ) di bawah pencahayaan simulasi solar.

# DISPERSION OF IRON OXIDE NANOPARTICLES ON OXIDE NANOTUBE FOR NANOCATALYST SYSTEM

## ABSTRACT

TiO<sub>2</sub> nanotube arrays (TNTs) and ZrO<sub>2</sub> nanotube arrays (ZNTs) were successfully fabricated by anodization in ethylene glycol (EG) containing 0.5 wt % NH<sub>4</sub>F at 60 V for 30 min. For the formation of nanotubes; oxidation and dissolution have been identified as two most important processes. The dissolution process occurs at the surface of the oxide, inside the pores and in between pores. Comparing TNT and ZNT; it appears ZNTs are longer with smaller diameter and thinner wall compared to TNT. Even though the anodic layer on Zr has higher value of polarization resistance (~3.92 kΩ) than TNTs (~7.82 kΩ) the dissolution rate of ZrO<sub>2</sub> is lower (0.11 mm/year) compared to TNTs (0.416 mm/year), making TNTs are shorter. The dissolution rate of oxide on Ti and Zr is also different resulting in different dimensions. Photocurrent and charge distribution measurement exhibited excellent ability of photogenerated free charge-carriers flow in TNTs but low for ZNTs. Therefore TNTs was need as a cathode to electrodeposit iron oxide. The formation of TNTs was further studied by the use of different oxidants (H<sub>2</sub>O, H<sub>2</sub>O<sub>2</sub> and KOH) added to the fluorinated-EG. KOH was revealed as the best oxidant to form nanotube arrays with a rate of ~ 254 nm min<sup>-1</sup> and was suitable to be used as a template for the electrodeposition of iron oxide. For the electrodeposition electrolyte consisting of 0.02 M FeCl<sub>3</sub>·6H<sub>2</sub>O + DI water was used. Parameters studied for this process included voltage, concentration of electrolyte and the effect of additives in the electrolyte. The growth mechanism of the nanoparticles and their morphology were described. From electron microscopy images, it is clearly observed that the presence of fine nanoparticles on the TNTs substrates were obtained

in electrolyte added with glycerol. Higher distribution of particles was observed with increasing potential applied to the cathode foil. Size and shape of the particles was also a function of the voltage. The average diameter of the spherical particles prepared at  $-1$  V was  $\pm 41.7$  nm. Increasing the voltage to  $-3$  V resulted in particles exhibit rice-like morphology with the average diameter and length are  $\pm 44$  nm and  $130$  nm, respectively. X-ray diffraction (XRD) and Raman spectroscopy measurements showed that the nanoparticles consisted of magnetite ( $\text{Fe}_3\text{O}_4$ ), maghemite ( $\gamma\text{-Fe}_2\text{O}_3$ ) and hematite ( $\alpha\text{-Fe}_2\text{O}_3$ ) after annealing at  $450^\circ\text{C}$  for  $2$  h (air). Photodegradation measurement confirmed the photocatalytic properties of hybrid photocatalyst system fabricated.  $\sim 90\%$  degradation of metal orange (MO) was observed on the TNTs|iron oxide system which is higher than that in pristine TNTs ( $\sim 75\%$ ). Photocurrent and Mott-Schottky measurement exhibited that the sample has the highest photocurrent generated ( $\sim 35 \text{ mA cm}^{-2}$ ) under solar simulator.

## CHAPTER 1

### INTRODUCTION

#### 1.1 Introduction

Environmental problems due to the rapid development of industrialization and population growth have become crucial issues in the world wide. The combustion of fossil fuel from transportation and industry, hazardous waste effluent coming out of residential, agricultural and industrial sectors, and contaminated ground water cause an unprecedented onslaught of deadly for aquatic and human life. Malato *et al.*, (2009) reported that 1.2 billion people have clean drinking water problem, while 2 billion people have no or little supplied of sanitized water and millions of people died every year due to the adverse effect of dirty water. It has been reported that only one half of clean water can be assessed from 1% of the entire water source in the world (Han *et al.*, 2009). It is anticipated that this problem may have been much increased in 2013. Seeing this various techniques are indeed required to be developed fast for purification of drinking water. There are many typical waste and contaminations in water for examples heavy metals, inorganic compounds, organic pollutants, and many other complex compounds (Li and Davis, 2009).

The removal of organic pollutants in wastewater is an important measure in ensuring clean water not only for human but for animals and aquatic life as well. Several methods have currently been employed for water treatment process such as activated carbon adsorption, physical and chemical technique, biological treatment and by the use of photocatalytic reaction via advanced oxidation processes (AOPs). For most of these processes, even though they are rather efficient and are suitable for certain application, they also possess disadvantages such as high energy consumption, the need of large systems or the use of chemical that can cause secondary

contamination (Gupta *et al.*, 2006). Moreover, some of the techniques are not suitable for certain more persistent organic pollutants (Atul *et al.*, 2013). This is to say that even after the process has been carried out, some of the organic pollutants still remain.

AOPs are well known methods for water treatment as AOPs can be used to degrade and mineralize organic pollutants (Jantawasu *et al.*, 2009). There are several ways that AOPs can be initiated; one of it is by the use of semiconductor heterogeneous photocatalyst. Semiconductor heterogeneous photocatalysis is the one of the versatile low-cost and high efficiency AOPs technologies (Oliveira *et al.*, 2010). Heterogeneous photocatalysis can be described as the acceleration of photoreaction in the presence of a photocatalyst (Ibhadon and Fitzpatrick, 2013). In heterogeneous photocatalysis two or more phases are used in the photocatalytic reaction. A light source is used to initiate the photoreaction. It is known that a semiconductor material will promote electrons from the valence band to the excited states in the conduction band if the material is illuminated by photons having energy greater than or equal to its band gap. The generation of electron and hole pair will lead to the formation of hydroxyl radical ( $\bullet\text{OH}$ ) and superoxide radical ( $\text{O}_2^{\bullet-}$ ) whereby they are the primary oxidizing species in the AOPs. The catalysts induce oxidations and reductions simultaneously. Nowadays semiconductors such as  $\text{TiO}_2$ ,  $\text{ZrO}_2$ ,  $\text{Fe}_2\text{O}_3$ ,  $\text{ZnO}$ ,  $\text{GaP}$ ,  $\text{CdS}$ , and  $\text{ZnS}$ , have been employed in heterogeneous photocatalysis (Morales-Flores *et al.*, 2011, Casbeer *et al.*, 2012).

In photocatalytic process, since the process gradually breaks down the contaminant molecules, no residue of the original material remains and therefore no sludge requiring disposal to landfill is produced. The catalyst itself is unchanged during the process and no consumable chemicals are required. These results in considerable savings and a simpler operation of the equipment involved. Additionally,

because the contaminant is attracted strongly to the surface of the catalyst, the process will continue to work at very low concentrations allowing sub part-per-million content to be achieved. Taken together, these advantages mean that the treatment process using photocatalyst results in considerable savings in the wastewater treatment production cost (Al-Rasheed, 2005). Moreover when the photocatalyst is made in nanoscale it is anticipated that the catalytic reactivity of the material would have been much improved. There have been works reported on the use of for example on nanoparticles or nanotubes of  $\text{TiO}_2$  as photocatalyst for waste water treatment (Fujishima and Honda, 1972). The use of nanomaterial can also opened up the possibility of the formation of smaller wastewater reactor compared to the existing treatment plant of wastewater treatment.

$\text{TiO}_2$  has been widely used as photocatalyst material since the discovery of its water splitting properties by Fujishima and Honda, 1972. But even so, the limitation such as high recombination of photogenerated electron-hole pairs and low visible light photosensitivity due to large band gap energy ( $E_g = 3.2\text{eV}$ ) are its significant obstacles (Benedix *et al.*, 2000). There are several ways in curbing the known problems with  $\text{TiO}_2$ . One of it is to combine  $\text{TiO}_2$  with a material with smaller energy gap forming a so-called hybrid nanostructured catalysts. In this work, iron oxide was selected as narrow-gap semiconductor due to good catalytic activity (Beydoun *et al.*, 2000).

Iron oxide material which is stable through a large pH range and, in general, it is considered to be extremely a stable material. Iron oxide is plentiful, cheap to manufacture and nontoxic. Iron oxide semiconductors exhibit a band gap of  $\sim 2\text{ eV}$ , which is small enough to collect a significant fraction of solar radiation. However, there are several drawbacks to iron oxide when it is used as a photoelectrode alone, such as low mobility of charge carriers due to a hopping mechanism of charge transfer



(Beermann *et al.*, 2000). Thus by coupling iron oxide and TNTs, better photocatalyst can be produced.

Hybrid nanostructure is defined as nanostructure consisting of two different nanomaterials with different morphologies. A combination of these different nanomaterials with different morphologies may result in much better photocatalytic properties thus suitable for organic pollutant degradation. This hybrid system is termed “nanophotocatalyst system”. It is consisted of iron oxide nanoparticles on TNTs. In this thesis, TNTs are in the form of thin film with nanotubular structure made by anodic process. Iron oxide nanoparticles were dispersed on them by electrodeposition process. Figure 1.1, a schematic of the hybrid photocatalyst system is shown. This figure is showing the top view of the system.

In a photocatalyst system, a support needs to have a high surface area, to which catalyst in a form of nanoparticles is affixed (Macak *et al.*, 2005a, Li *et al.*, 2013).

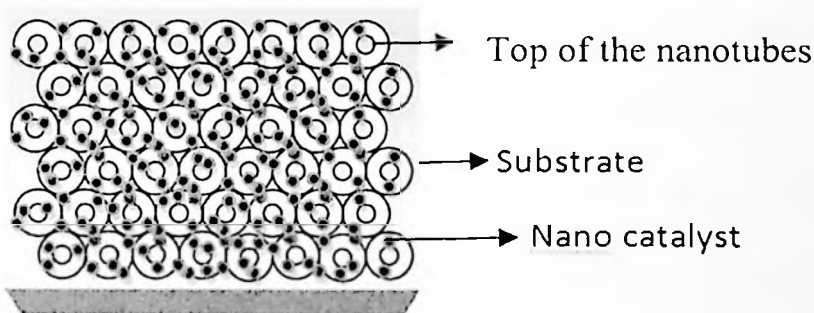


Figure 1.1. Illustration of a structured photocatalyst system

Seeing the importance of this hybrid system, this thesis focuses on the fabrication of it. Even though there are several works on the formation of nanotubes on Ti, not many works have been extended to produce hybrid iron oxide-TiO<sub>2</sub> system. This is indeed what was done in this work but focus was given on the methods of the formation of both nanotubes and the nanoparticles. A simple, cost effective and very efficient process was selected; electrochemical process. In here, nanotubes were created by

anodic process and the nanoparticles were produced by electrodeposition process. For the nanotubes formation, experiments were conducted on effect of the electrolyte composition to the final morphology of the oxide. The main aim was to find an electrolyte which can produce nanotubes at as short time as possible and can also be recycled for several experiments. And as for the electrodeposition process, the main experiment was conducted on the effect of voltage and additive to the formation behaviour of the iron oxide nanoparticles.

## 1.2 Problem statement

This research was conducted to produce well-aligned  $\text{TiO}_2$  and  $\text{ZrO}_2$  nanotube arrays to be used as a template whereby the iron oxide nanoparticles will be dispersed on top. To obtain well-aligned nanotube arrays, Ti and Zr foils were anodized in fluoride organic electrolyte. Anodization process can be defined as well-desired electrochemical growth of an oxide layer on a metal substrate by polarizing the metal anodically in an electrochemical cell. Anodization can be done by three different modes; potentiostatic, galvanostatic and potentiodynamic mode (Pasquale et al., 2002). And among others, potentiostatic anodization appears as the most suitable mode for the formation of self-ordered nanotubular structure both on Ti and Zr due to its extreme simplicity (Roy *et al.*, 2011, Mohapatra *et al.*, 2007). Organic electrolyte like ethylene glycol (EG) has been investigated as electrolyte of choice for the formation of such nanotubular arrays. However the availability of the oxygen in EG is considered difficult because it is strongly bound to the carbon atom by a double bond (Raja *et al.*, 2007). Removal of the oxygen from carbon to react with the metal surface is therefore unlikely. However, as mentioned EG is relatively hygroscopic and tends to take up considerable amounts of water from environmental air. Oxidation of Ti is then

Although  $\text{TiO}_2$  has many advantages, there are two main obstacles that hinder its practical applications which are 1) the low quantum yield of photo-oxidation reaction of  $\text{TiO}_2$  attributed to the fast recombination electrons and holes pairs, and 2) low activity under visible light (Saliby *et al.*, 2011, Tong *et al.*, 2008). In order to improve the property of  $\text{TiO}_2$ , hybrid system consisting of iron oxide on  $\text{TiO}_2$  was created in this work. Even though there have been reported works on the use of this system for photocatalyst process, not a lot have been done on the electrochemically driven nanoparticles. Therefore, it is of interest to investigate on how electrochemically derived iron oxide nanoparticles on  $\text{TiO}_2$  nanotubes would have on the photocatalytic ability. As for the case of  $\text{ZrO}_2$  as template, in this work, experiments were done to explore the capability of this oxide as photocatalyst then to decide if indeed it can be used as template for iron oxide formation. As will be explained in chapter 4, despite extremely high aspect ratio of nanotubes formed on Zr, the oxide produced small photocurrent which can be translated to poor photocatalyst. Moreover the oxide is not very good conductor hence iron oxide nanoparticles deposition was much more difficult.

Iron oxide nanoparticles were deposited onto the  $\text{TiO}_2$  nanotube arrays by electrodeposition methods. Despite a lot of works been done on the formation of iron oxide on flat substrate but not many has been reported the formation of the iron oxide on nanotubular substrate as template for the iron oxide formation. Therefore in this work hybrid nanotube arrays (iron oxide|TNTs) was fabricated via electrodeposition to gain much information regarding the formation behaviour of iron oxide nanoparticles on the nanotube surface and the factors affecting it.

The final stage of the experiment was to evaluate the photocatalytic activity of hybrid material in order to explore the possibility of using this photocatalyst system for photocatalyst, photo electrochemical and chemical reactor applications.

### 1.3 Objectives

The objectives of the research are:

1. To compare the formation behavior and structural characteristic of TNTs and ZNTs nanotubes in fluoride EG by current density-time and potentiodynamic measurements.
2. To investigate the effect of  $\text{H}_2\text{O}$ ,  $\text{H}_2\text{O}_2$  and KOH in the anodic electrolyte on the growth of TNT.
3. To investigate the electrochemical deposition process of iron oxide on TNTs as to produce hybrid nanostructure.
4. To evaluate the properties of Iron oxide|TNTs in term of its PEC, PC and Mott-Schottky properties

### 1.4 Thesis outline

This thesis is organized in to five chapters. Consequently, in chapter 1, a brief introduction, problem statement and objective of the research are elaborated. Chapter 2 begins by laying out the comprehensive review of metal oxide nanotube. The properties, method of synthesis and factor affecting geometry of nanotube are elaborated. The fundamental concepts of nanostructured catalyst system formation by electrodeposition and photocatalyst are also discussed in details. A brief explanation on the applications is presented. The final part elaborates a comprehensive review on

the enhancement of photocatalytic activity by loading of iron oxide on TiO<sub>2</sub> nanotube arrays.

Chapter 3 deals with the experiment procedures that were used in this study. These include the experimental design and the preparation of TiO<sub>2</sub> and ZrO<sub>2</sub> nanotube arrays by anodization as well as the formation of hybrid nanostructure by using electrodeposition techniques. The characterization techniques of nanotube arrays are included. These comprise of a brief explanation on the characterization equipment, their operation principles and sample preparation.

Chapter 4 presents the experimental results and comprehensive discussion on the formation behaviour of TiO<sub>2</sub> and ZrO<sub>2</sub> nanotube arrays via anodization in fluoride EG and evaluate their properties using potentiodynamic polarization as well as the formation of hybrid nanostructure by using electrodeposition. This chapter consists of main three parts, including: 1) the detail investigation on the growth behaviour of TiO<sub>2</sub> and ZrO<sub>2</sub> nanotube arrays and the effect of their structural characteristics on their properties, 2) the enhancement of the growth of the nanotube arrays by incorporating alkali material (KOH) and other oxidants: H<sub>2</sub>O and H<sub>2</sub>O<sub>2</sub>, and 3) the formation of hybrid photocatalyst comprising the nanotube arrays as support with iron oxide nanoparticles dispersed on the tubes by electrodeposition approach and the assessment of the photocatalytic activity of this hybrid system. Finally, chapter 5 is devoted to the conclusions of this research work and suggestions for the future work.

## CHAPTER 2

### LITERATURE REVIEW

#### 2.1 Introduction

A review presented in this chapter is aimed at providing a better understanding regarding the three main materials investigated in this thesis:  $\text{TiO}_2$ ,  $\text{ZrO}_2$  and  $\text{Fe}_2\text{O}_3$ . The first two materials were produced by anodic process and were studied in this work for support (or template) material whereas the  $\text{Fe}_2\text{O}_3$  in the form of nanoparticles were dispersed by electrodeposition on the surface of this support to produce hybrid nanostructure. This chapter is divided into two main parts; the first part is on anodization technique, and properties of anodized valve metal oxide nanotube arrays. The second part is on the mechanism of hybrid nanostructure formation, the advantages and properties aiming at gathering understanding on the electrodeposition process of  $\text{Fe}_2\text{O}_3$ .

#### 2.2 Valve metal oxide

##### 2.2.1 Metal oxide nanotube arrays

Valve metals are mainly transition group metals which can be oxidised to form a thin anodic oxide on their surfaces. Transition metals are element whose atom has an incomplete d sub-shell, or which can give rise to cations with an incomplete d sub-shell (Cox, 2010). Oxides grown on transition metals are transition metal oxides or (valve metal oxide) and it is well known that transition metal oxides have many interesting properties.  $\text{TiO}_2$  and  $\text{ZrO}_2$  are transition metal oxides.  $\text{TiO}_2$  occurs as a mineral in the nature while pure mineral of  $\text{ZrO}_2$  is rare in nature and most of Zr occurs as zircon ( $\text{ZrSiO}_4$ ). Many features of these valve metal oxides become useful and feasible if the material is in micro-or nanostructures specifically when they exhibits a

high surface area which may enhance many of their surface related properties. Various research works are now focusing on the design and control to produce thin film of transition metal oxides with nanostructures via various synthesis strategies. The nanostructured film of oxides can be synthesized by chemical approaches. The most typical approaches are sol–gel and hydrothermal approaches or processes which are based on chemical vapour processes like chemical vapour deposition process. The morphologies that can be produced from these processes include nanofilms or films with nanostructures: nanowires, nanorods and nanotubes or films comprising of nanocrystallites.

Electrochemical process is a chemical route to form thin film with nanostructures. Electrochemical process can be done anodically or cathodically. Anodic process often results in the formation of oxide on metal foil (anodic oxidation). Anodic process needs an electrochemical bath containing the necessary electrolyte, anode (metal to be oxidised) and cathode (often Pt rod is used). Anodic current or potential is applied to the anode and oxidation will take place at the surface of the metal accordingly. Through anodic oxidation the formation of oxide film comprising of aligned, ordered nanotubes can also be formed covering the surface of metal anode homogeneously optimised (Roy *et al.*, 2011). In anodic process regardless of the size of the metal foil such 3-D network of nanotubes can be fabricated on its surface. Nonetheless, there are various parameters that must be optimized in order to produce nanotubes with uniform dimension, that can cover the whole area of the metal foil uniformly and all including anodization potential, electrolyte composition and properties thereof (conductivity, viscosity), as well as anodization time and temperature. In this work, as the surface of the materials to be used as a template for the dispersion of  $\text{Fe}_2\text{O}_3$ , the homogeneity of the length and the tube diameter is needed.

To achieve this, anodization parameters were studied. Therefore, works done by other researchers on the topic of nanotubes formation by anodization is reviewed here. The introduction on the properties of the three oxides investigated:  $\text{TiO}_2$ ,  $\text{ZrO}_2$  and  $\text{Fe}_2\text{O}_3$  will however be given first.

#### **2.2.1.1 Properties of $\text{TiO}_2$ nanotubes**

Since the first discovery of ordered, aligned nanotubes of  $\text{TiO}_2$  on Ti by Gong *et al* in (2001), anodic  $\text{TiO}_2$  nanotubes have received significant attention since they have shown extraordinary properties. The nanotubes have large number of diverse advanced applications including sensors (Varghese *et al.*, 2004, Mor *et al.*, 2004), dye sensitized solar cells (Mor *et al.*, 2006), hydrogen generation by water photoelectrolysis (Mor *et al.*, 2008, Grimes *et al.*, 2008), photocatalytic reduction of  $\text{CO}_2$  under outdoor sunlight (Varghese *et al.*, 2009), photoelectrochemical water splitting and supercapacitors (Fabregat-Santiago *et al.*, 2008). In addition,  $\text{TiO}_2$  nanotubes have demonstrated significant benefit in biomedical applications, including in biosensors applications, in molecular filtration, in drug delivery and tissue engineering (Popat *et al.*, 2007, Liu and Chen, 2005, Xie *et al.*, 2007, Peng *et al.*, 2009).  $\text{TiO}_2$  exists in three natural crystalline phases: rutile, anatase and brookite. Generally the properties of  $\text{TiO}_2$  depend on the crystallinity and isomorphs type of the oxide, and therefore the usefulness of the application also varies. For instance, anatase phase is preferred to be used in charge-separating devices such as dye-sensitized solar cells (DSSCs) and as photocatalyst, while rutile is used primarily in gas sensors and dielectric layers. Rutile is the room temperature stable phase of  $\text{TiO}_2$  (Santos *et al.*, 2009). However, as-fabricated  $\text{TiO}_2$  nanotube arrays is known to be amorphous and it can be transformed into crystalline phases during annealing at elevated temperatures.



Generally, crystallization or phase transformations of  $\text{TiO}_2$  nanotubes take place through nucleation and growth processes (Kondo and Domen, 2007). Varghese *et al.*, (2003) investigated crystallinity transformation of  $\text{TiO}_2$  nanotube arrays prepared by anodic process by using Glancing Angle X-Ray diffraction (GAXRD) as shown in Figure 2.1. From Figure 2.1, it is obvious that the sample annealed at 230-250 °C is still amorphous and only titanium peak observed. Anatase phase begins to form at temperature somewhere between 250-280°C. The anatase grain size initially increases with temperature, decreasing between ~480°C and 580°C, then again increasing beyond 580°C. At around 430°C, rutile phase begins to appear. Rutile formation occurs specifically at the nanotubes Ti support interface region leaving the anatase crystallite in the walls unaffected. This could be due to the oxidation of the Ti layer. Rutile grain size progressively increases with temperature after its nucleation. As the annealing was done at higher temperature between 480 and 580°C, both Ti and larger anatase crystals at the interface can be directly transformed into rutile. Complete transformation from anatase to rutile occurs in the temperature range 620–680°C. Further increasing of the annealing temperature to 820°C resulted in the changes of the tubular structure whereby it would be disturbed, even though at some points, porosity remained with the walls of the nanotubes coalesced to form a worm-like appearance.

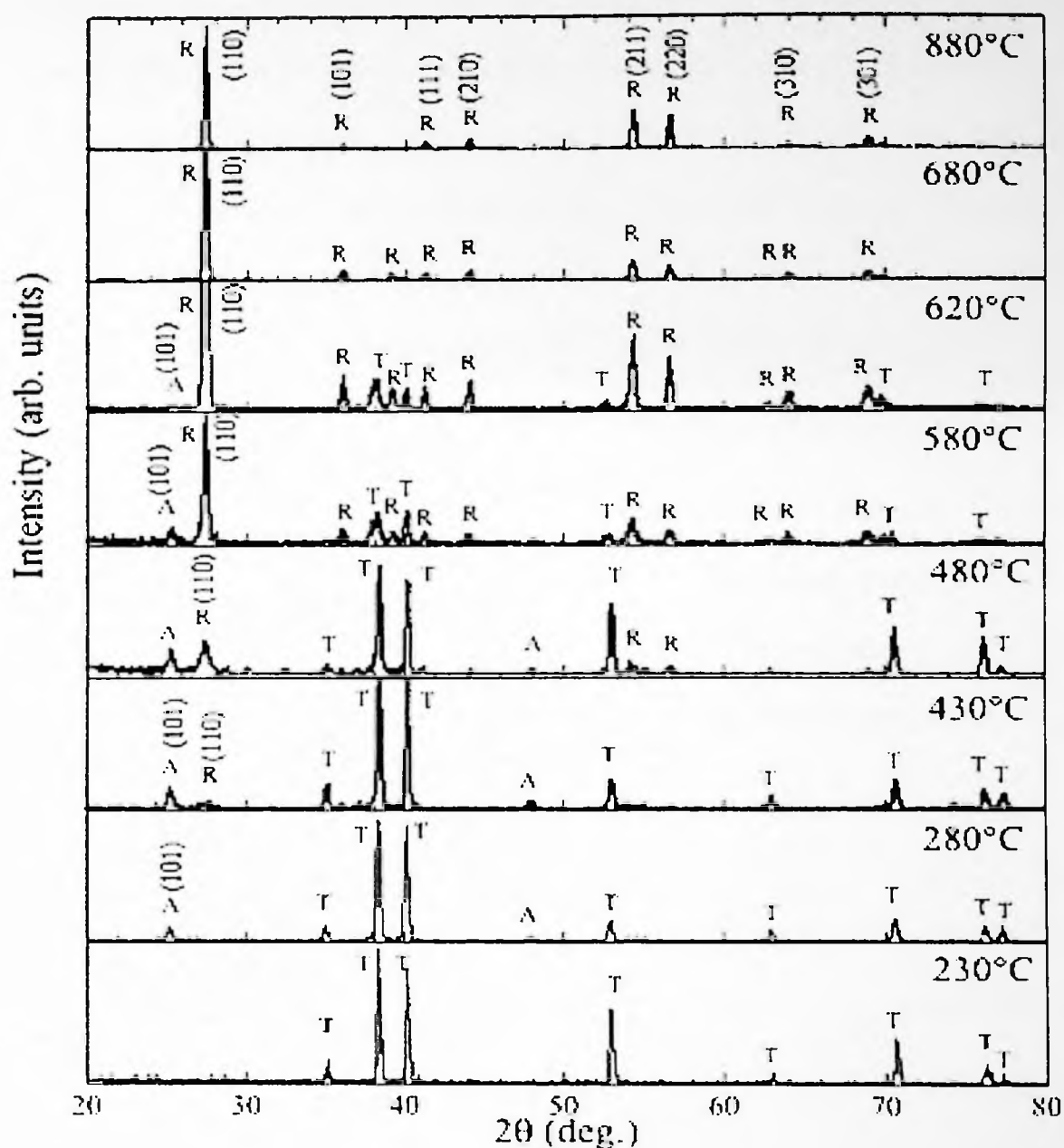
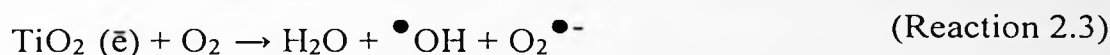


Figure 2.1 Glancing angle X-ray diffraction (GAXRD) patterns of  $\text{TiO}_2$  nanotube arrays annealed at temperatures range from 230 to 880°C for 3 h. A, R, and T represent anatase, rutile, and titanium, respectively (Varghese et al., 2003).

Other than XRD, Raman spectroscopy can also be used to investigate the crystallinity of  $\text{TiO}_2$  nanotube arrays.  $\text{TiO}_2$  nanotubes have 6 Raman active modes for anatase; which can be identified at  $144\text{ cm}^{-1}$ ,  $197\text{ cm}^{-1}$ ,  $399\text{ cm}^{-1}$ ,  $513\text{ cm}^{-1}$ ,  $519\text{ cm}^{-1}$ ,  $639\text{ cm}^{-1}$  and 4 for rutile at  $143$ ,  $447$ ,  $612$  and  $825\text{ cm}^{-1}$  (Qian et al., 2005).

Khatae *et al.*, (2010) reported that the percentage of anatase and rutile phases in the oxide effect the photocatalytic performance of the oxide thus knowledge on the phases of the TiO<sub>2</sub> is needed. TiO<sub>2</sub> is a semiconductor oxide with wide band gap of 3.0 - 3.2 eV. It is known that a semiconductor material will promote electrons from the valence band to the excited states in the conduction band if the material is illuminated by photons having energy greater than or equal to its band gap ((2.1). The generation of electron and hole pair leading to the formation of hydroxyl radical (OH<sup>•</sup>) and superoxide radical (O<sub>2</sub><sup>•-</sup>) ((2.2 and (2.3) whereby they are the primary oxidizing species in the photocatalytic oxidation process (AOP). The detailed mechanism of this process was proposed by Fujishima *et al.*, in (2000). The oxidative reactions of the OH<sup>•</sup> with various organic molecules would result in the degradation of the organic pollutants:



Anatase has band gap of 3.2 eV, corresponding to UV wavelength of 385 nm. Pure anatase exhibits lower rates of recombination of electron and holes in the oxide in comparison to rutile due to its 10-fold greater rate of hole trapping (Riegel and Bolton, 1995). Rutile has a smaller band gap of 3.0 eV with excitation wavelengths that extend into the visible at 410 nm. Moreover, pure phase rutile is photocatalytically inactive. It has been established that rutile exhibits high rates of recombination in comparison to anatase (Hurum *et al.*, 2005). Moreover the adsorptive affinity of

anatase for organic compounds is higher than that of rutile (Stafford *et al.*, 1993). This answer why the anatase is the best phase for photocatalyst application as mentioned before. This is also supported by several authors whereby they agreed that anatase is better for this application (Hirakawa *et al.*, 2007, Malinger *et al.*, 2011).

#### **2.2.1.2 Properties of ZrO<sub>2</sub> Nanostructure**

Zirconium dioxide (ZrO<sub>2</sub>) is a technologically important engineering material that can be used not only in structural ceramics but also in advanced application. For instance ZrO<sub>2</sub> has been used as catalyst and catalyst support because of its good physicochemical properties, surface acidity and reactivity (Yamaguchi, 1994). ZrO<sub>2</sub> is also known to have high ionic conductivity hence is useful as oxygen conductor. It has been used in solid oxide fuel cell and as oxygen sensor (Tan and Wu, 1998). ZrO<sub>2</sub> can exist as three polymorphs: monoclinic (M), tetragonal (T) and cubic (C). Based from calculation, the band gap of monoclinic, tetragonal and cubic ZrO<sub>2</sub> are computed to be 3.12-5.4 eV, 4.10-13.3 eV and 3.2-12.3 eV respectively (Chang and Doong, 2007). The band gap of ZrO<sub>2</sub> obtained from experimental technique is still controversial because of different microstructures, method of formation and chemical composition of ZrO<sub>2</sub> obtained will give different values. To investigate the energy gap of ZrO<sub>2</sub> experimentally, two techniques are often used: photoluminescence and UV-Visible spectroscopy. Berlin *et al.*, (2012) described three kinds of processes responsible for the luminescence of ZrO<sub>2</sub>: (i) band to band recombination (ii) recombination at impurity levels and (iii) recombination at intrinsic defects. From the band to band luminescence band gap of ZrO<sub>2</sub> can be determined.

Similar to TiO<sub>2</sub>, determination on the phases in ZrO<sub>2</sub> has been done by XRD and Raman spectroscopy method. However when ZrO<sub>2</sub> is in nanoscale, XRD has a

limitation since peaks from the XRD of nano-sized particles are very broad. Raman shifts for T-ZrO<sub>2</sub> are reported at 147, 270, 314, 480 and 642 cm<sup>-1</sup>. Broad band of 177-188 cm<sup>-1</sup> is the characteristic for M- ZrO<sub>2</sub> and peaks at 350 and 470cm<sup>-1</sup> also belong to M-ZrO<sub>2</sub>. Raman shift for C-ZrO<sub>2</sub> is at 633cm<sup>-1</sup> (Kontoyannis and Orkoula, 1994) and several authors reported that C-ZrO<sub>2</sub> has a rather amorphous-like Raman spectrum with broad band at approximately 530-670 cm<sup>-1</sup>. This is due to the symmetry of cubic phase. HRTEM has also been used to investigate the crystallinity of nanoparticles of ZrO<sub>2</sub> (Tahir *et al.*, 2007). Crystallinity can be identified by looking at lattice fringes in the HRTEM image. The lattice fringes can provide information of the d spacing ( $d_{hkl}$ ) of the phase (Lee and Smyrl, 2005, Tahir *et al.*, 2007).

Besides having good ionic conductor properties, apparently ZrO<sub>2</sub> also can be used as photocatalyst as reported by Sayama & Arakawa (1996) that ZrO<sub>2</sub> has been successful to decompose toxic and organic compounds in polluted water and air. They claimed that the oxide semiconductor has a wide band gap and highly negative flat-band potential which is adequate in water splitting process. And this was confirmed by Reddy *et al.* (2003) who reported that T and M-ZrO<sub>2</sub> can successfully split water with contribution of T-ZrO<sub>2</sub> is slightly better compares to M-ZrO<sub>2</sub>. Karunakaran and Senthilvelan (2005) also used ZrO<sub>2</sub> particles as photocatalyst for the oxidation of aniline. Nanocrystalline ZrO<sub>2</sub> for degradation of Rhodamine dye was done by Zheng *et al.* (2009). However, the use of ZrO<sub>2</sub> nanotubes as photocatalyst has not been reported apart from Zhao *et al.* (2011) and Wang *et al.* (2012) for the degradation of MO and alcohol respectively.

### 2.2.2 Synthesis Metal Oxide Nanotube arrays by Anodization

TiO<sub>2</sub> nanotubes have been fabricated through various methods such as sol-gel (Daoud and Xin, 2012), hydrothermal (Yu and Yu, 2008), chemical vapor deposition (Hsieh *et al.*, 2010) and anodization techniques (Gong *et al.*, 2001, Choi *et al.*, 2004, Macak *et al.*, 2006b). On the other hand ZrO<sub>2</sub> can be formed by template techniques and anodization as well. Among these methods, anodization has been recognized as one of the most attractive routes to fabricate self-aligned ordered TNT arrays in one step despite annealing is required to crystallise the oxide as mentioned before Figure 2.2 shows a typical anodization set up as reported by Roy et al. (2011).

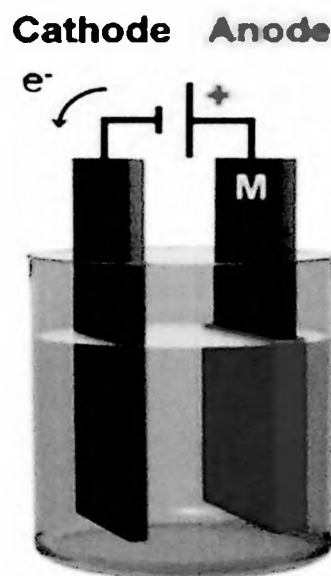


Figure 2.2 Illustrative drawing of a two-electrode electrochemical cell in which the valve metal are anodized. (Roy et al., 2011)

### 2.2.3 Factor affecting geometry and composition

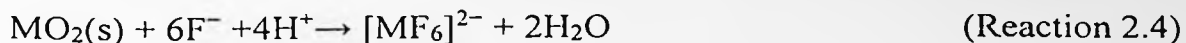
The anodic growth of tubular structure is well known as the equilibrium reaction between electrochemical (anodic) oxidation at the metal/electrolyte interface and chemical dissolution at the oxide/electrolyte interface the dissolution of the oxide will

results in the formation of porous film which will then be transferred to nanotubular structure. The geometrical features of nanotube arrays are controlled through various synthesis parameters, including electrolyte composition (Macak *et al.*, 2005b, Yoriya *et al.*, 2007, Shankar *et al.*, 2007), electrical potential (or current) applied to the anode (Paulose *et al.*, 2006) and anodization time (Shankar *et al.*, 2007). This section presents a review of the effect of these parameters on the formation of oxide nanotube arrays.

#### **2.2.3.1 Effect of Electrolyte composition (nanotube arrays synthesis using organic electrolyte)**

Electrolyte plays an important role in the formation of  $\text{TiO}_2$  on Ti foil by anodization process. Anodization of Ti can lead to the formation of compact oxide layers, so called barrier-type anodic oxides, or porous oxides in the form of nanopores, nanotubes (ordered or disordered layers), mainly depending on the electrolyte used as reviewed by Kowalski *et al.* (2013) as shown in Figure 2.3. On Zr, nanotube can be formed as well but the morphology is not as clear as TNTs as reported by Schmuki *et al.* (2006).

To produce nanotubular oxide, the electrolyte needs to have fluorine inside it. According to Valota *et al.*, the fluorine will react with  $\text{TiO}_2$  by chemical dissolution as well as the incorporation of the F inside the cell boundaries of the growing porous structure would results in the formation of  $\text{F}^-$  rich layer. This fluoride rich layer has to be dissolved in water to create a good separation between pores forming discreet nanotubes as shown by (2.4). The reaction is also applicable to the formation of  $\text{ZrO}_2$  nanotube arrays. M represents either Ti or Zr.



The formation of  $\text{TiO}_2$  nanotube arrays was first achieved by anodic oxidation of a Ti foil in aqueous hydrofluoric acid (HF) electrolyte (Gong et al., 2001). However, high chemical dissolution at the top of the nanotubes by strong acidity of HF aqueous electrolyte limits the applied potential to as low as in the range of 5 – 20 V. This consequently limits the nanotube length as ~500 nm. Macak et al. (2005d) suggested that the abundant amount of  $\text{F}^-$  and  $\text{H}^+$  in HF dominates high chemical dissolution and thus hinders the equilibrium growth of nanotube arrays. After the development of nanotubes in this so called first generation electrolyte,  $\text{TiO}_2$  nanotube arrays up to 10  $\mu\text{m}$  were produced in fluoride ion-containing buffered solution (sodium sulphate added with NaF for example). Then a third generation electrolyte which is based on organic electrolyte was introduced whereby nanotubes with length in few hundred microns were produced. The nanotubes were produced in baths in combination with a variety of non-aqueous organic polar electrolytes, including dimethyl sulfoxide (DMSO), formamide (FA), ethylene glycol (EG) and N-methylformamide (NMF) (Ruan et al., 2005; Paulose et al., 2006; Shankar et al., 2007). Organic electrolyte is termed third generation electrolyte. The simplicity of anodization process in fluorinated organic electrolyte does not require the application of potential ramp due to high resistivity of organic solvent as compared to water (Ruan et al., 2005, Paulose et al., 2006). As for  $\text{ZrO}_2$ , works done on this have been reported by Kowalski et al., (2013) as well.



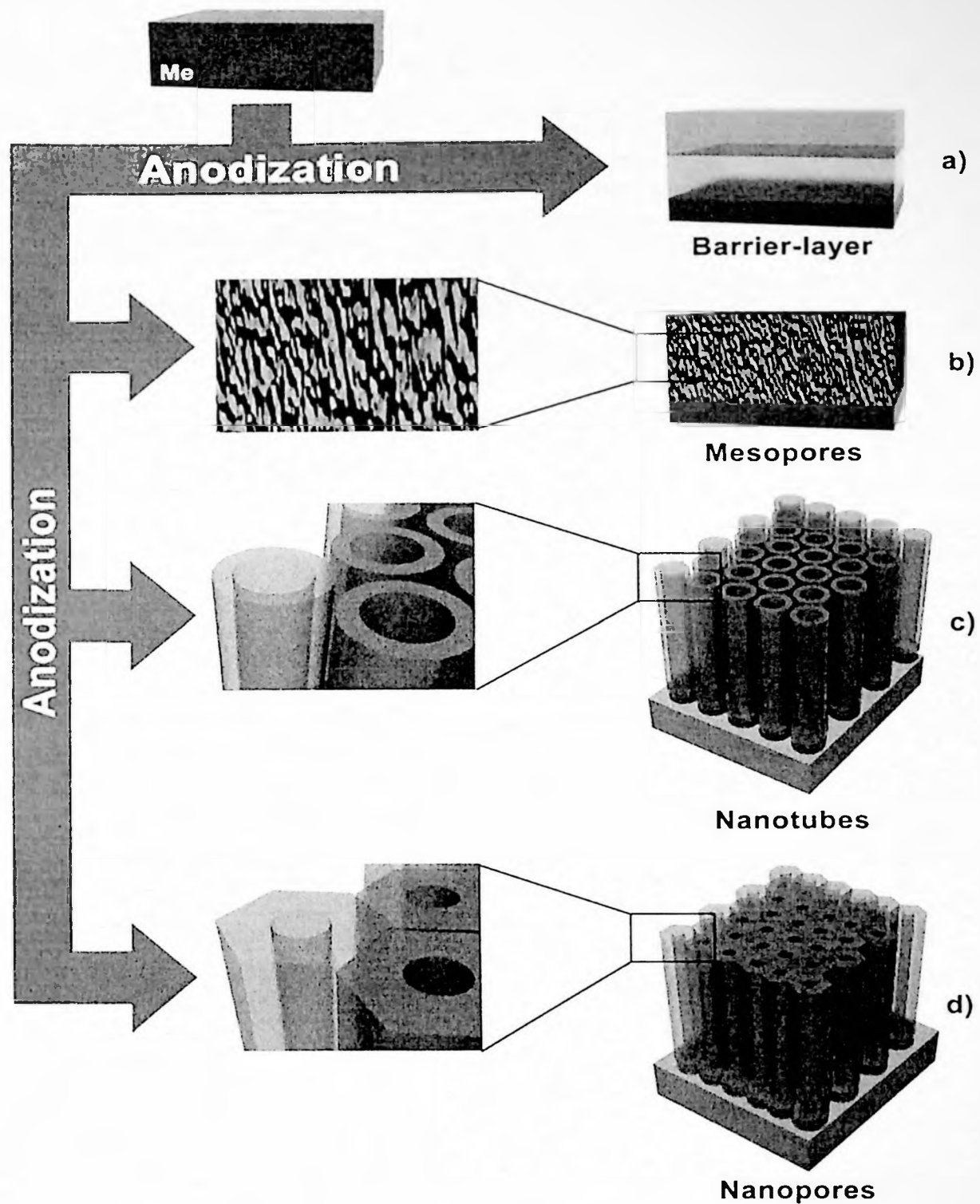


Figure 2.3 Different morphologies of the oxides obtained by anodization of transition metals in various electrolytes: (a) barrier type-oxide can be formed in most of the aqueous electrolytes, (b) mesosponge, microcones, nanochannels formed in hot-glycerol phosphate electrolyte, (c) nanotubes formed in fluoride electrolytes, and (d) oxide with open porous character (Kowalski *et al.*, 2013).

The increase in the length of the nanotube formed in fluoride organic electrolyte is due to the reduction of chemical dissolution of the anodic oxide at the surface but local dissolution is maintained at the bottom of the nanotubes, inside the tube at the electrolyte|oxide interface. The dissolution here is needed to produce elongated pores which form the long channel. At the same time, anodization will happen at the barrier layer inside the pore, which will increase the amount of H. This produces low pH region inside the nanotubes which would increase the rate of etching.

Yoriya *et al* (2007) considered that the existence of organic component in the electrolyte modifies the space charge region in the tubes and thus reducing the lateral etching, forming a steady pore growth and lowering etching of the nanotube walls. This allows the nanotube to grow deeply into Ti substrate without significant loss from the pore mouth. The incorporation of organic component in the oxide is also known to lower the relative permittivity of oxide and increase its dielectric breakdown potential (Antony *et al.*, 2012), therewith allowing the anodic growth of oxide under wide range of applied potential (Alivov *et al.*, 2009, Shankar *et al.*, 2007). Due to this larger diameter nanotubes can be produced.

In 2006, Paulose *et al* demonstrated the fabrication of well-aligned TiO<sub>2</sub> nanotube arrays using various electrolytes including 1.5wt% H<sub>2</sub>O with 0.3-0.6wt% of NH<sub>4</sub>F in FA/NMF, 0.25wt% NH<sub>4</sub>F in EG and 2wt% HF in DMSO. The longest nanotube arrays with the length of approximately 134  $\mu\text{m}$  were obtained through anodization in EG electrolyte containing 0.25wt% NH<sub>4</sub>F. Shankar *et al.* (2007) further investigated the formation of TiO<sub>2</sub> nanotube arrays by the variation of H<sub>2</sub>O and ammonium fluoride in EG electrolyte. Anodization in EG containing 2wt% H<sub>2</sub>O and 0.30wt% NH<sub>4</sub>F resulted in the well-aligned TiO<sub>2</sub> nanotube arrays up to 220  $\mu\text{m}$  within 17h. The formation of nanotube with growth rate of 308.3 nm.min<sup>-1</sup> was achieved by

anodization in EG electrolyte which containing 5wt%  $\text{NH}_4\text{F}$  and 1wt%  $\text{H}_2\text{O}$  (Sreekantan *et al.*, 2010). From here, it is obvious that EG has shown a potential to attain long nanotubes with high aspect ratio (Paulose *et al.*, 2006). Moreover, the anodic-oxidation in EG induced the adsorption of carbon species on the nanotube walls, thereby enabling visible-light absorption (Mohapatra *et al.*, 2007) without further processing (Park *et al.*, 2006). This is to say that doping of C can also be done when organic electrolyte is used.

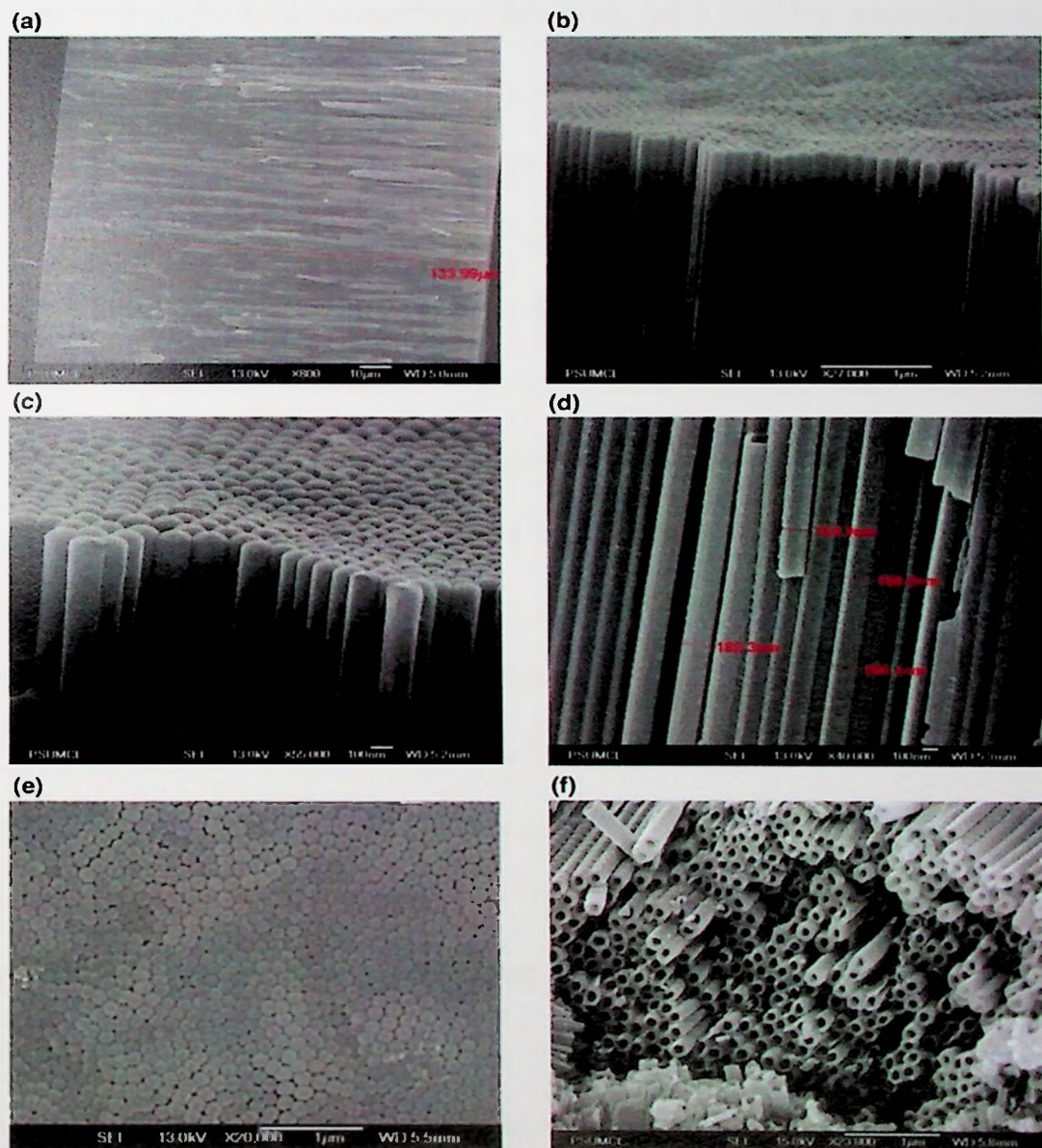


Figure 2.4 FESEM images of a nanotube arrays grown in ethylene glycol containing 0.25wt %  $\text{NH}_4\text{F}$  at 60 V showing (a-d) cross-sectional views at varying degrees of magnification, (e) view of bottom surface and (f) top surface (Prakasam *et al.*, 2007)



Even though EG can be used as the electrolyte to produce TiO<sub>2</sub> nanotubes, but the donation of O<sub>2</sub><sup>-</sup> in organic electrolyte is seen to be more difficult than that in aqueous electrolyte. Since the O<sub>2</sub><sup>-</sup> is strongly bonded to the carbon with double bonding, the oxidation in EG is slow. To overcome this, water is usually added as the source of O<sub>2</sub><sup>-</sup> and OH<sup>-</sup> (Paulose *et al.*, 2007) for oxidation to happen. Moreover, according to Yoriya *et al.* (2007), the addition of small amount of water to EG can improve the adhesion between the nanotube and underlying oxide barrier layer. This facilitates the growth of long nanotubes. However, the excessive amount of water in the electrolyte will decrease the viscosity of EG and lead to the high chemical dissolution at the top of nanotube due to the high diffusion rate of reactant ions here (Macak *et al.*, 2006a, Prakasam *et al.*, 2007). Paulose *et al.* (2006) considered that the amount of water concentration that can be tolerated to keep the rate of dissolution on the surface not faster than that on the bottom of nanotube and thereby allowing the nanotube to grow deeply into the metal without significant loss at the tube mouth is no more than 5 wt %. A larger amount of water will result in high dissolution rate on the surface and causes short tube.

Another really important reason for water in EG is to allow the pore separation process that will distinguish the nanotubular structure with porous structure (Valota *et al.*, 2009). It is known that fluoride species migrate inward about twice as fast as O<sub>2</sub><sup>-</sup> ions, and accumulate at the pore boundaries. The F<sup>-</sup> rich layer will be dissolved leading to nanotubes formation. (Valota *et al.*, 2009) pointed out that water will enhance the dissolution of this F<sup>-</sup> rich layer.

Apart from water peroxide H<sub>2</sub>O<sub>2</sub> can also be used as the oxidant in fluoride EG. However there are not many works reported on the use of H<sub>2</sub>O<sub>2</sub> in fluoride EG as oxidant apart from Sreekantan *et al.* They reported on the fabrication of well-aligned